



Quantification of surface area and intrinsic mass transfer coefficient for ultrasound-assisted dissolution process of a sparingly soluble solid dispersed in aqueous solutions

Krishna Sandilya Durbha, Kannan Aravamudan *

Department of Chemical Engineering, Indian Institute of Technology Madras, Chennai 600036, Tamil Nadu, India

ARTICLE INFO

Article history:

Received 24 March 2011

Received in revised form 17 September 2011

Accepted 26 September 2011

Available online 1 October 2011

Keywords:

Particle breakage

Ultrasound

Particle size characterization

Lognormal distribution

Interfacial area

Intrinsic mass transfer coefficient

ABSTRACT

The efficacy of power ultrasound of 20 kHz in enhancing the volumetric mass transfer coefficient was investigated in this study. Breakage and dissolution of sparingly soluble benzoic acid dispersed in either water or 24% aqueous glycerol was monitored as a function of time and ultrasound power input. Particle size measurements were carried out at intermediate times during the experiment to estimate the mean particle size and surface area. Linear combination of lognormal distributions was found to fit the experimental particle size distribution data. The De Brouckere mean diameters (d_{43}) obtained from the particle size distributions decreased with increase in the ultrasonic power level. Empirical correlations were developed for the evolution of surface area as a function of ultrasonic energy input per unit mass. The effect of ultrasound on the intrinsic mass transfer coefficient (k_c) could be decoupled from the volumetric mass transfer coefficient ($k_c a$) as the surface area was also estimated. Different approaches involving either constant or variable intrinsic mass transfer coefficients were employed when carrying out the delineation. Mass transfer rates were enhanced due to both higher ultrasound induced intrinsic convective mass transfer coefficient and additional surface area created from particle breakage. To delineate the effects of particle breakage from solid dissolution, experiments were also carried out under non-mass transfer conditions by pre-saturating the solvents with benzoic acid. Both the solid–liquid systems examined in the present study attained saturation concentration when the ultrasonic energy input per unit mass was approximately 60 kJ/kg, irrespective of the ultrasonic power level setting.

© 2011 Elsevier B.V. All rights reserved.

1. Introduction

Solid dissolution is an important industrial process which has several multi-disciplinary applications. A batch solid–liquid mass transfer process is modeled by the following equation:

$$\frac{dC}{dt} = k_c \left(\frac{S}{V} \right) (C^* - C) \quad (1)$$

Factors such as concentration driving force, interfacial area and the intrinsic mass transfer coefficient affect the rate of dissolution of solid in a solvent as apparent from Eq. (1). These require intensification in situations where the solid is sparingly soluble. The versatility of ultrasound intensification of engineering processes has been firmly established previously [1,2]. It potentially can influence all the parameters in Eq. (1) viz. the intrinsic mass transfer coefficient (k_c), interfacial area (S/V) and the concentration driving force for mass transfer ($C^* - C$). Hence it is necessary to resolve the

volumetric mass transfer coefficient ($k_c S/V$) to delineate the effects of ultrasound on the intrinsic mass transfer coefficient and interfacial area for mass transfer. In a previous study by Thompson and Doraiswamy [3] it was claimed that ultrasound could induce significant supersaturation in the dispersion whereby higher mass transfer rates could be obtained. Sandilya and Kannan [4] found that for the benzoic acid based aqueous systems involving water and 24% (w/w) glycerol, the apparent supersaturation was induced by the uncontrolled temperature rise arising from ultrasonic energy dissipation in the dispersion. Once the temperature was well controlled, the apparent supersaturation effect disappeared. In this study, the effect of acoustic cavitation on the remaining parameters viz. intrinsic mass transfer coefficient (k_c) and surface area (S) are explored.

When the solid particles dispersed in a liquid are exposed to power ultrasound, they are effectively fragmented. Further, the ultrasound field creates intense mixing of the particles in the dispersion [4]. These phenomena involving creation of more surface area as well as enhanced convection could be exploited to intensify the mass transfer rates in sparingly soluble systems. Studies involving the effect of power ultrasound on simultaneous size

* Corresponding author. Tel.: +91 44 2257 4170; fax: +91 44 2257 4152.

E-mail address: kannan@iitm.ac.in (K. Aravamudan).

Nomenclature

a	correlation parameter in Eqs. ((6) and (7)), cm^2 (or) cm^2/g	t^*	time taken by solid–liquid system to reach saturation, s
A_i	blend factor of lognormal distribution, %	u	velocity scale, m/s
b	correlation parameter in Eqs. ((6) and (7))	V	volume of solvent, m^3
B_i	standard deviation of lognormal distribution, m	<i>Greek letters</i>	
c	correlation parameter in Eqs. ((6) and (7))	α	correlation parameter in Eq. (11a)
C	concentration of solute in aqueous solution, mol/m^3	β	correlation parameter in Eq. (11a)
C^*	saturation limit of sparingly soluble solute, mol/m^3	γ	correlation parameter in Eq. (11a)
C_i	mean of lognormal distribution, m	δ	characteristic energy input per unit mass required to attain saturation, kJ/kg and used in Eqs. ((6) and (7))
d_{43}	De Brouckere mean diameter, m	ϕ	volume of particles in a particular size interval, %
d_p	average particle size, m	Φ	sphericity of particles, –
$d_{p,i}$	average particle size of i th fraction, m	μ	viscosity of solvent, Pa s
D_{AB}	diffusivity of solute (A) in solvent (B), $\text{m}^2 \text{s}^{-1}$	ν	kinematic viscosity, m^2/s
k_c	intrinsic mass transfer coefficient, m/s	ρ	density of solvent, kg/m^3
$k_c a$	volumetric mass transfer coefficient, s^{-1}	ρ_p	density of particles, kg/m^3
k_{US}	intrinsic mass transfer coefficient in presence of ultrasound, m/s	<i>Subscripts</i>	
l	length scale, m	Expt	related to experiment
m_i	mass of particles in i th fraction, kg	Pred	predicted values
Re	Reynolds number, –	<i>Abbreviations</i>	
Re_{US}	Reynolds number based on specific energy dissipation rate = $\frac{d_{43}^{4/3} \epsilon^{1/3}}{\nu}$, –	EM	energy input per unit mass, kJ/kg
S	surface area, m^2	MT	mass transfer conditions
S'	specific surface area, m^2/g	NMT	non-mass transfer conditions
Sc	Schmidt number = $\frac{\mu}{\rho D_{AB}}$, –	SA	surface area, cm^2
Sh	Sherwood number = $\frac{k_c d_{43}}{D_{AB}}$, –	SSA	specific surface area, cm^2/g
Sh_{US}	Sherwood number in presence of ultrasound = $\frac{k_{US} d_{43}}{D_{AB}}$, –	US	ultrasound
t	time, s		

reduction and dissolution of particles are scarce in open literature. Lu et al. [5] studied the effect of power ultrasound (20 kHz) on dissolution and particle size reduction in the context of contaminated sediment treatment. Sandilya and Kannan [4] presented briefly the volumetric mass transfer coefficients obtained under ultrasound assisted solid dissolution. There are also a few papers pertaining to the ultrasound-assisted solid–liquid chemical reactions [6,7]. Ratoarinoro et al. [6] observed a significant size reduction of potassium hydroxide particles in a solvent (toluene) under sonicated conditions. Hagenson and Doariswamy [7] monitored the particle size reduction of sodium sulfide when it reacted with liquid benzyl chloride in the presence of ultrasound. They reported that the mean size of sodium sulfide particles was reduced from 40 to 16 μm during 15 min of reaction in presence of sonication at 20 kHz. Ultrasound is utilized effectively in the field of leather processing as well. Sivakumar et al. [8] could reduce the particle size of lime from 38,299 to 1790 nm during the liming process of ultrasound assisted leather treatment.

In literature, the surface area variation in the presence of ultrasound was treated either in the presence of a chemical reaction or in the absence of mass transfer [7,9,10]. But studies addressing the effect of ultrasound on the creation of surface area in a solid (dispersed)–liquid system in the presence of mass transfer alone are very limited. While mass transfer may occur rapidly in the presence of ultrasound, it may also concomitantly lead to loss in surface area due to complete dissolution of particles and creation of smaller particles from larger ones. These effects have to be delineated from the non-mass transfer effects which only involve particle fragmentation and breakage. Hence the surface areas created under identical operating conditions such as time of sonication, frequency and ultrasonic power in a given system may still be quite different depending on whether or not the particle breakage

is accompanied by solid dissolution. This differentiation may become important in the design of ultrasound intensified mass transfer equipment for dispersed systems. The estimation of the intrinsic mass transfer coefficient (k_c) instead of just the volumetric mass transfer coefficient ($k_c S/V$) in the presence of ultrasound enables the estimation of Sherwood number which will be useful in the design of suitable mass transfer equipment for process intensification. A few studies have reported the effect of ultrasound on the intrinsic mass transfer coefficient during phase transfer catalyzed reactions [6,11]. In the present study, the effect of ultrasound on solid–liquid mass transfer was studied by conducting experiments with benzoic acid particles dispersed in different aqueous solvents. The effect of the ultrasound on particle size reduction in these systems was also studied in the absence of mass transfer.

2. Materials and methods

2.1. Materials

Benzoic acid particles as received from HiMedia, Mumbai (AR grade) were sieved to give an average feed particle size of 1800 μm (size range of sieves: $-2 +1.6 \text{ mm}$; DIN standards) in all the runs. AR grade glycerol (Ranbaxy Fine Chemicals Limited, New Delhi) and distilled water were used to prepare 24% (w/w) aqueous glycerol solution. The distilled water aqueous solution is termed as System 1 and the 24% (w/w) glycerol system is termed as System 2 for the sake of brevity in the following discussions. Using two different systems enabled the variation in viscosity and hence the Schmidt number dimensionless group. The properties of these two systems are provided in Table 1.

Table 1
Physical properties of the systems used in the preset study at 30 °C [4].

Item number	Solvent	Saturation limit of benzoic acid (g/L)	Density (kg/m ³)	Viscosity (cp)	Diffusivity of benzoic acid × 10 ⁹ (m ² /s)	Sc (–)
1	Distilled water	4.04	996	0.85	1.12	762
2	24% (w/w) glycerol	4.44	1054	1.76	0.54	3098

2.2. Experimental setup

Particle breakage studies were carried out in a jacketed stainless steel cylindrical vessel. A cryostat (Ultra Cryostat Circulator, Scientific Instruments, Chennai, India) was used to maintain isothermal condition. An ultrasonic probe (model VCX-500, Sonics and Materials Inc., USA), rated at 500 W with a resonating frequency of 20 kHz and a tip diameter of 13 mm was used to induce ultrasonic waves in the process vessel. The particle size distributions at each experimental combination of ultrasonic power level setting and sonication time are measured using a laser particle size analyzer (model S3500, Microtrac Inc., USA), which has a measuring range from 0.025 to 1408 μm.

2.3. Experimental procedure

Two types of experiments were carried out to investigate the effect of ultrasound. In the first, ultrasound-assisted particle breakage experiments were carried out in the presence of mass transfer which occurred through solid dissolution. Pure solvent was used at the beginning of these runs so that particle sizes were influenced by simultaneous breakage and dissolution until saturation conditions were attained. After saturation, the particle sizes will be reduced only by breakage. In the second type of experiments, particle size reduction occurs in the complete absence of mass transfer and hence only through breakage right from the beginning of the experiment. For this purpose, a separate set of experiments was carried out where the distilled water or the 24% (w/w) aqueous glycerol solvent was *pre-saturated* with benzoic acid so that solid dissolution is prevented right at the outset. These were termed as non-mass transfer runs.

In a typical run, (either with or without mass transfer), 10 g of solute was charged as feed into the process vessel containing 800 mL of solvent. Actually, the solubilities of benzoic acid in the solvents used were not high. The concentration of 10 g per 800 mL is about 2.8–3.1 times the saturation loading as may be seen from the C^* values given in Table 1. In the earlier work of Sandilya and Kannan [4] this concentration level was chosen in order to check for occurrence of any supersaturation in the presence of ultrasound. Hence, the same amount of feed for particle breakage experiments was continued in the present work as well to maintain consistency. This concentration level also further ensured that sufficient number of particles with a wide size range were still present in dispersion even after saturation conditions have been attained.

The ultrasonic probe was positioned at the centre of the process vessel and ultrasonic generator was switched on at a desired power level setting to initiate the run. Two levels of ultrasonic power input expressed as a percentage of maximum setting were used in continuous sonication mode. The ultrasonic power level was applied in the continuous mode at 50% and 70% of maximum setting. The actual power dissipated in each solid–liquid system as a function of percentage setting was quantified using calorimetry studies [7]. The setting of the ultrasonic device (50% and 70%) is mentioned for easier comprehension of the percentage of maximum power possible that was applied to a particular run. However, in the correlation developed for surface area and the parameter estimation calculations involved in the Sherwood

number correlation, the actual power dissipated as obtained from calorimetric experiments were used. The actual power dissipated as determined from calorimetric measurements at different operating conditions is provided in Table 7 and also captioned in Figs. 2 and 3. At 50% and 70% power level settings used in the present work, the particles were found to be suspended and well dispersed for both the systems studied.

The time of sonication varied between 3 and 45 min depending on the power level setting. The contents of process vessel were maintained at 30 ± 1 °C by means of a cryostat. Sonication was switched off after a predetermined duration of time and the process vessel contents were analyzed for particle size distribution. In case of non-mass transfer experiments the concentration of the solute was monitored in the middle and at the end of each run and it was found that there was no change from the saturated state. This ensured that the initial concentration (i.e., saturation concentration of benzoic acid in distilled water for this illustration) was maintained constant throughout the duration of the experiment and that the particle size reduction was only due to ultrasonic irradiation. After sonication was switched off, samples were taken from the dispersion for each batch and each sample was analyzed twice for the particle size measurement. The average value of these measurements was then reported. The particle size analyzer reports the histogram of the volume distribution of particles (in percent) as a function of specified particle size intervals. The sphericity of benzoic acid particles was determined experimentally to be 0.60 using the image analysis technique. ImageJ[®] software was used to process the images of the particles taken in different orientations so as to estimate the surface area of the particles.

2.4. Characterization of particle size distributions

The specific surface area of each experimental combination was calculated from the respective particle size distribution using the following equation [12]:

$$S' = \left(\frac{6}{\rho_p \Phi} \right) \frac{\sum (m_i / d_{p,i})}{\sum (m_i)} \quad (2)$$

The particle size distribution data were analyzed for the lognormal distribution trends using the procedure outlined by Allen [13]. Data pertaining to every experimental condition was plotted on a log-probability graph and the modality of the distribution (i.e., unimodal/bimodal/trimodal) were identified. The lognormal distribution was fitted to the experimental data and the distribution parameters were obtained by using the *nlnsq* toolbox of Matlab (MATHEMATICS, 2007). The parameters obtained from the nonlinear regression approach were also confirmed with POLYMATH[®] software which uses the Levenberg–Marquardt algorithm. The multi-modal distribution was fitted using a linear combination of lognormal distributions [14–19]:

$$\frac{d\phi}{d(\ln d_p)} = \sum_{i=1}^n \frac{A_i}{B_i \sqrt{2\pi}} \exp \left(-\frac{[\ln(d_p) - C_i]^2}{2B_i^2} \right) \quad (3)$$

where ϕ represents the cumulative volume percentage of particles added at each interval up to the particle size d_p of interest. The LHS of Eq. (3) is termed as the “density function”. The differentiation in Eq. (3) was carried out numerically using the backward difference

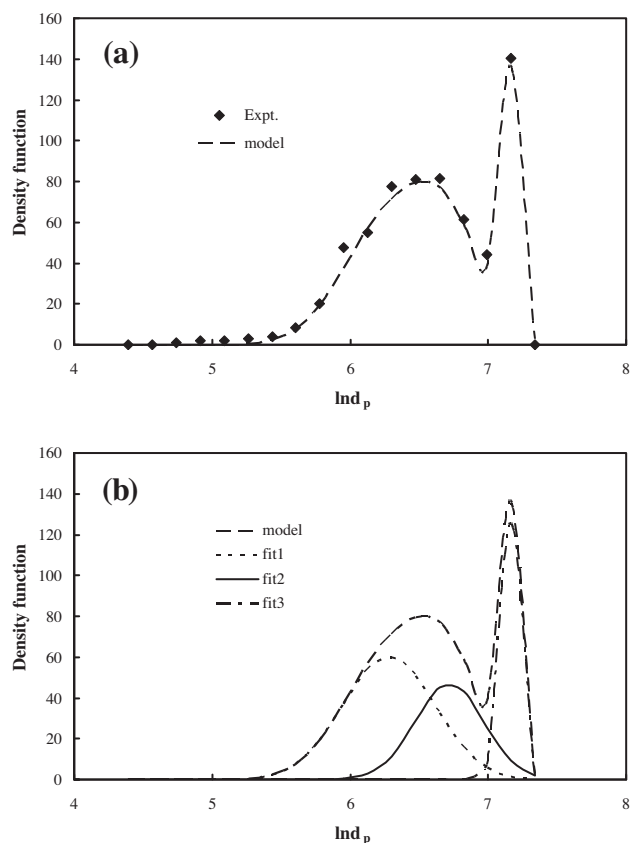


Fig. 1. (a) Comparison of experimental data and lognormal model of probability density functions for System 1 after 3 min of sonication at 70% power level setting under mass transfer conditions and (b) individual lognormal models that are blended to form the overall model for conditions in (a).

formula. The parameters of the model given by Eq. (3) viz. blend factor (A_i), standard deviation (B_i) and mean (C_i) were thus estimated for each experiment. They were then used to predict the overall distribution of the particles. A typical comparison of the experimental data and the lognormal model is illustrated in Fig. 1. Three intersecting distributions contributing for the overall trimodal distribution may be easily perceived from this figure. The contribution of each mode towards the overall tri-modal distribution in this case is quantified in terms of “percentage blend factors”. For the case depicted in Fig. 1, the first mode corresponding to smaller particle sizes contributes 60% towards to overall distribution whereas the second (medium size) and third (coarse size) modes hold a share of 28% and 12%, respectively. The lognormal distributions were found to fit the experimental data satisfactorily and R^2 value better than 0.97 in few cases and better than 0.98 in the remaining were obtained. The statistical parameters (A_i , B_i , C_i) of the fitted distribution is given in Table 2. The De Brouckere mean diameter (d_{43}) for the given particle size distribution is calculated using the following general equation [13,20,21].

Table 2
Fitted lognormal parameters for mass transfer (MT) case depicted in Fig. 1.

Run ID: PSAA6	Blend factor, A_i (%)	Standard deviation, B_i	Mean, C_i	R^2
Fit 1	59.56	0.356	6.305	0.995
Fit 2	27.81	0.262	6.773	
Fit 3	12.63	0.039	7.156	

$$d_{43} = \frac{\int_{\ln a}^{\ln b} (d_p \frac{d\phi}{d \ln d_p}) d \ln d_p}{\int_{\ln a}^{\ln b} (\frac{d\phi}{d \ln d_p}) d \ln d_p} \quad (4)$$

The limits $\ln(a)$ and $\ln(b)$ represent the natural logarithm of the lower and upper bounds of the experimental particle size distribution and varies from one run to another. The following analytical expression may be derived from Eq. (4) to obtain the d_{43} for each individual lognormal mode of the fitted multimodal particle size distribution [11,22]:

$$d_{43}|_{\text{individual}} = \exp \left(C_i + \frac{1}{2} B_i^2 \right) \quad (5)$$

2.5. Estimation of interfacial area and intrinsic mass transfer coefficients

The interfacial areas calculated from the particle size distributions were expressed empirically in terms of ultrasonic energy dissipated per unit mass of the dispersion. The appropriate correlation was embedded in the transient rate equation of solid dissolution (Eq. (1)). The resulting expression was numerically integrated using the ODE45 routine of MATLAB® (The MathWorks, Inc.). The unknown parameter k_c for each run involving mass transfer was estimated by minimizing the sum of squares of the deviations between experimental concentration–time data and numerical predictions. The parameter estimation was carried out using the *NONLINSQ* option of MATLAB®.

3. Results and discussion

First, the effect of ultrasound on average particle size is discussed in the presence and absence of mass transfer. The interfacial areas calculated from the experimental particle size distributions under mass transfer and non-mass transfer conditions are compared. Typical distributions are presented in Figs. 5–7 to support these discussions. The intrinsic mass transfer coefficients are then presented for both systems.

3.1. Effect of sonication time on particle size

The effect of ultrasonic energy dissipated into the particle dispersion on the De Brouckere mean diameter (d_{43}) is depicted in Fig. 2. The De Brouckere mean diameter (d_{43}) refers to the center of gravity of the volume distribution [23]. The actual power dissipated, as estimated from calorimetric measurements, are also given in the legends of Figs. 2 and 3. Theoretical predictions of d_{43} shown in Fig. 2 were obtained by using the blended lognormal model (Eq. (3)) in Eq. (4) and integrating between the appropriate limits.

As shown in Fig. 2a, particle breakage at 50% power level setting was not that effective as the cavitation events would be less intense than those at 70% power level setting. In case of 70% power level setting, the particle breakage was relatively more rapid. Benzoic acid in System 1 had reached 99% of its saturation concentration in 9 min when operated at 70% power level setting. After this time, there is a noticeable drop in the rate of particle size reduction. This rate-reduction may have been at least partially due to absence of any further significant dissolution and presence of more number of smaller particles created during solid dissolution.

After 6 min of operation at 70% power level setting, finer particles with sizes less than 100 μm were just getting generated. The cumulative mass fraction of such finer particles was 12% of total mass of particles at this juncture. This cumulative fraction of finer particles (<100 μm) increased to 30% after 9 min of sonication. All the medium sized particles were reduced to finer size after

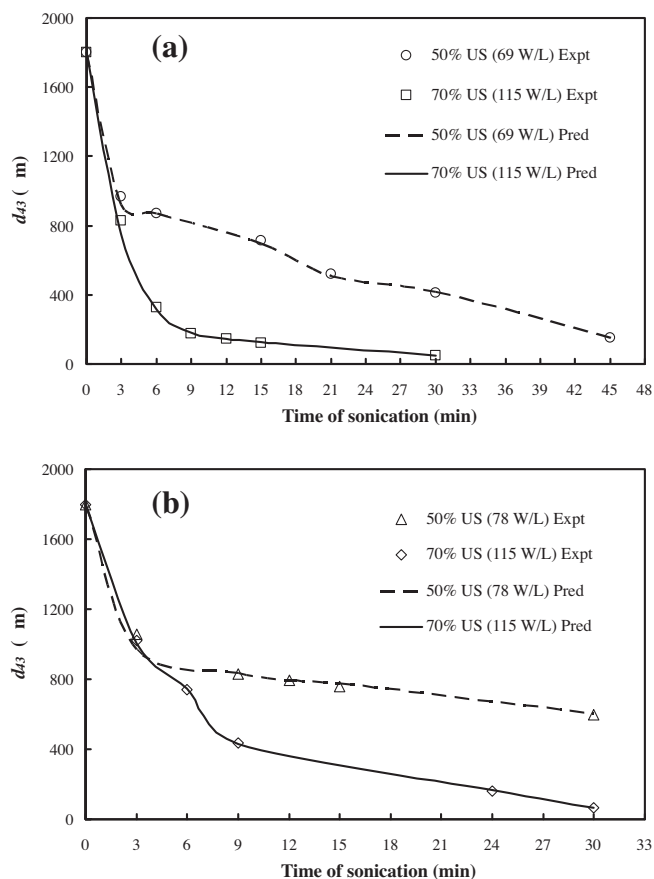


Fig. 2. Variation of d_{43} with respect to ultrasonic power level setting under mass transfer conditions: (a) System 1 and (b) System 2.

30 min of sonication. At this juncture, the cumulative mass fractions of particles of size less than 10 and 100 μm were 13% and 95%, respectively.

At 50% power level setting, the process of size reduction became slower after 3 min of sonication. Particles of sizes less than 100 μm just started generating after 15 min of sonication (1% of the total mass of particles at that moment). This cumulative fraction became somewhat considerable after 21 min of sonication viz. 5%. After 30 min of sonication, 13% by mass of the particles are of size less than 100 μm at this juncture. There are no particles present in the size range less than 10 μm even after 45 min of sonication at 50% power level setting. But the cumulative fraction of particles of size less than 100 μm is significant at this point in time (45%).

Based on the trends depicted in Fig. 2a it appears that there are three stages in the overall i.e., average particle size reduction. The initial stage may correspond mainly to the rapid coarse particle size reduction. The first stage occurs for about 3 min at both power dissipations in System 1. The second stage corresponds mainly to the intermediate particle size reductions while some coarser particles may also be breaking at this stage adding to the intermediate particle size range. At 70% power level setting, the second stage lasts between only 3 and 9 min. At 50% power level setting, the second stage appears to last for a longer time i.e., between 3 and 21 min, approximately. The third stage corresponds to the slowest rate of reduction of mainly smaller sized particles. It could be that very large particles are broken instantaneously upon exposure to ultrasound irrespective of the ultrasonic power level setting. However, for further breakage, ultrasonic power level dependent factors such as speeds of microjets, particle speeds in the dispersion (which influence inter particle collisions) and shockwaves may have greater say in average particle size reduction [7,24].

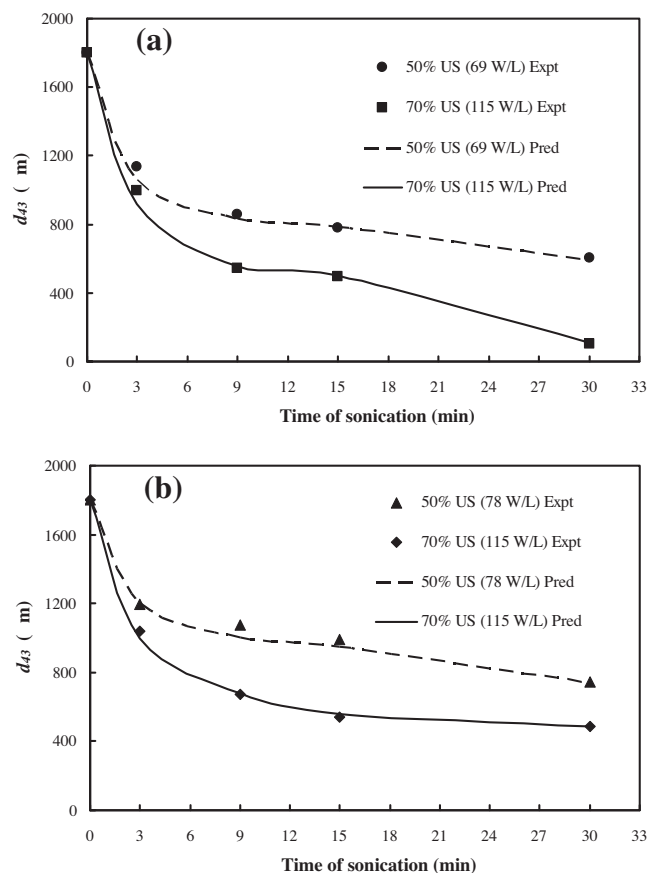


Fig. 3. Variation of d_{43} with respect to ultrasonic power level setting under non-mass transfer conditions: (a) System 1 and (b) System 2.

The particle size reduction in presence of mass transfer is a combined effect of particle breakage and solid dissolution. As may be seen from Fig. 2a, the reduction in d_{43} became gradual after the system attained saturation concentration when operated at 70% power level setting (i.e., after 9 min of sonication). For 50% ultrasonic power level setting, System 1 attained saturation concentrations only after 45 min and hence the d_{43} was seen to be continuously decreasing albeit somewhat slowly with respect to the time of sonication (Fig. 2a). This confirms that the solid dissolution also plays an important role in particle size reduction until the system attains saturation concentration.

Fig. 2b depicts the influence of ultrasonic power level setting on the d_{43} for System 2 in the presence of mass transfer. For System 2 the time taken to attain saturation at 50% power level setting was 15 min while it was 9 min at 70% power level setting. At 70% power level setting, there was a decrease in the particle size reduction rate after 9 min of sonication. However at 50% power level setting, there was no discernible change in the average particle size reduction rate after the initial rapid decrease during the first 3 min of sonication. Hence it appears that at low power level setting, the effect of solid dissolution in reducing particles of intermediate sizes is not very significant. This may be explained also by lower rates of solid dissolution at low power level setting in high viscous system which may hence lead to slower rate of particle size reduction even when saturation conditions have not been attained. Solid dissolution also requires higher convection along the solid–liquid interface which is enabled at higher power level settings and lower solvent viscosities.

Fig. 3a and b illustrate the variation of d_{43} for Systems 1 and 2 at different ultrasonic power level settings under non-mass transfer conditions, respectively. The particle size reduction for System 1

was not rapid as it was in presence of mass transfer even at 70% ultrasonic power level setting, the highest power level setting used in the present investigation (Fig. 3).

For System 2, the particle breakage was not significant, even at a power level setting of 70% (Fig. 3b). Higher viscosity of System 2 may have hindered the effects of cavitation and hence the particles were not broken easily.

3.2. Evolution of surface area under mass transfer and non-mass transfer conditions

The particle size distribution data obtained from the laser particle size analyzer was processed to determine the specific surface area generated as a result of size reduction of particles. The methodology was outlined in Section 2.4. The average sphericity of particles obtained from batches of experiments conducted under different process conditions (ultrasonic power level setting and time of sonication) was found to be 0.60. The sphericity of crushed particles generally varies between 0.60 and 0.80 [12]. The average value of sphericity measured in this work (0.60) was used to calculate the experimental values of surface area (SA) and specific surface area (SSA).

Empirical correlations for SA and SSA were developed as a function of ultrasonic energy input per unit mass (EM) using nonlinear regression feature of POLYMATH® software. It was found for both Systems 1 and 2, at an ultrasonic energy input per unit mass of around 60 kJ/kg, near saturation concentrations of the solute in the respective solvents were attained. For System 1 at 70% power level setting, this value of EM (60 kJ/kg) corresponds to 9 min of sonication and the concentration of benzoic acid had reached 99% of its saturation concentration by then (Table 3). In the case of 50% power level setting it took 15 min for System 1 to reach

an EM value of 60 kJ/kg and the concentration of benzoic acid at that juncture was quite close (94%) to saturation concentration. In case of System 2 at 70% ultrasonic power level setting, the system reached 99% of saturation concentration when the ultrasonic energy input per unit mass was 58 kJ/kg, which corresponds to 9 min of sonication. It may be seen from Table 3 that System 2 had attained 99% of saturation concentration after 15 min of sonication at 50% power level setting. This corresponded to an energy dissipation of 58 kJ/kg.

Once the system reaches saturation concentration the particle size reduction is a sole result of particle breakage. Hence, empirical correlations for surface area and specific surface area were developed in two phases: the first phase corresponds to both solid dissolution and particle breakage (i.e., until the system had reached saturation concentration) and the second takes care of breakage alone (i.e., after the system had reached saturation concentration). The general form of the correlations developed for the evolution of surface area (SA) and specific surface area (SSA) with energy input per unit mass (EM) under mass transfer and non-mass transfer conditions are given in Eqs. ((6) and (7)), respectively. The corresponding values of these correlation parameters are given in Tables 4 and 5, respectively.

$$SA \text{ (or) } SSA = a + b (EM)^c \quad \text{if } EM \leq \delta \quad (6a)$$

$$SA \text{ (or) } SSA = a + b (EM - \delta)^c \quad \text{if } EM > \delta \quad (6b)$$

$$SA \text{ (or) } SSA = a + b (EM)^c \quad (7)$$

where δ is the value of EM required for the solid–liquid mass transfer system to reach near saturation concentration.

Fig. 4 compares the SA of particles generated in Systems 1 and 2 as a result of sonication for both mass transfer and non-mass

Table 3
Characteristics of different solid–liquid systems studied during ultrasound-assisted solid dissolution.

Solid–liquid system	Ultrasonic power level setting (% of maximum)	δ (kJ/kg)	Time taken by the system to reach an EM of δ (min)	Fraction of saturation concentration attained by the system (%)	d_{43} Of solid particles (μm)
Benzoic acid–distilled water	50	60	15	94	714
	70	60	9	99	177
Benzoic acid–24% (w/w) aqueous glycerol	50	66	15	99	760
	70	58	9	99	438

Table 4
Values of correlation parameters developed for the estimation of SA and SSA under mass transfer conditions.

Solid–liquid system	US power setting (%)	δ (kJ/kg)	EM (kJ/kg)	SA (mass transfer) (cm^2)			SSA (mass transfer) (cm^2/g)		
				<i>a</i>	<i>b</i>	<i>c</i>	<i>a</i>	<i>b</i>	<i>c</i>
Benzoic acid–distilled water	50	60	≤ 60	413.34	157.78	0.31	41.33	13.23	0.50
			> 60	977.12	2.62	1.56	143.77	0.38	1.56
	70	60	≤ 60	413.34	4.52	1.64	41.33	0.74	1.62
			> 60	4170.0	2.36	1.84	612.00	0.37	1.83
Benzoic acid–24% (w/w) aqueous glycerol	50	66	≤ 66	413.34	158.27	0.23	41.33	14.28	0.44
			> 66	835.00	2.62×10^{-6}	4.68	140.00	2.29×10^{-8}	5.37
	70	58	≤ 58	413.34	0.07	2.44	41.33	0.07	1.98
			> 58	1767.0	4.26×10^{-3}	3.42	271.33	7.11×10^{-5}	3.41

Table 5
Values of correlation parameters developed for the estimation of SA and SSA under non-mass transfer conditions.

Solid–liquid system	US power setting (%)	SA (non-mass transfer) (cm^2)			SSA (non-mass transfer) (cm^2/g)		
		<i>a</i>	<i>b</i>	<i>c</i>	<i>a</i>	<i>b</i>	<i>c</i>
Benzoic acid–distilled water	50	413.34	53.38	0.69	41.33	5.33	0.69
	70	413.34	0.18	2.09	41.33	0.02	2.09
Benzoic acid–24% (w/w) aqueous glycerol	50	413.34	36.58	0.70	41.33	3.66	0.70
	70	413.34	18.84	1.01	41.33	1.88	1.01

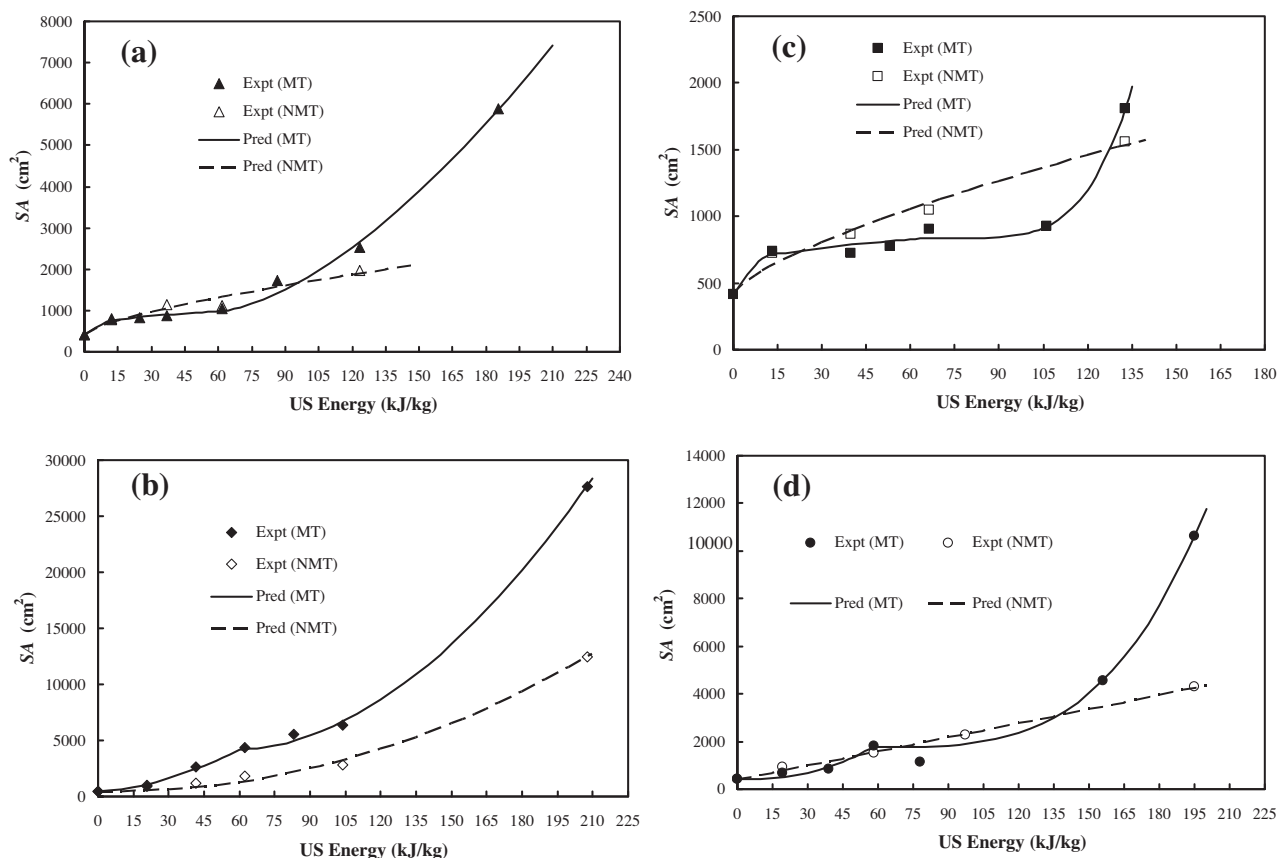


Fig. 4. Comparison of surface areas created under mass transfer (MT) and non-mass transfer (NMT) experiments for (a) System 1 at 50% power level setting, (b) System 1 at 70% power level setting, (c) System 2 at 50% power level setting and (d) System 2 at 70% power level setting.

transfer cases. The predicted values of SA from empirical correlations given in Tables 4 and 5 are also plotted in Fig. 4. It may be seen from Fig. 4 that for both systems, the SA increased with respect to ultrasonic energy applied per unit mass both under mass transfer and non-mass transfer conditions. For mass transfer conditions, the inflection in the SA trend observed at an EM value of around 60 kJ/kg for both 50% and 70% power level settings demarcates the unsaturated conditions from the nearly saturation concentration conditions.

The surface area trends for different systems and power level settings are discussed below.

3.2.1. 50% power level setting for System 1

Under mass transfer conditions, the increase in SA for System 1 was relatively slow until saturation, and then it becomes more rapid as there is no disappearance of particles due to dissolution henceforth (Fig. 4a). In the presence of solid dissolution, SA rise is slow as the surface area increase by breakage may have been partially negated by a loss in SA due to loss of particles by dissolution. Once near saturation conditions were obtained, these particles did not dissolve as rapidly as before and the surface area began to increase. The rapid increase in the surface area may be attributed to creation of more surface area from existing moderate sized particles by the sonication. More number of smaller sized particles (<100 μm) also began to get generated after 15 min of sonication. These particles also did not dissolve rapidly in the solution anymore as saturation concentration has been nearly reached. Further breakage of these smaller particles also contributes to rapid rise in surface area. On the other hand, under non-mass transfer conditions, the existence of still moderate sized particles which

have not yet broken into numerous smaller particles cause the surface area to increase only monotonically and gradually (Fig. 4a).

3.2.2. 70% power level setting for System 1

As shown in Fig. 4b, the increase in surface area during mass transfer run at 70% ultrasound power level setting is higher when compared to the corresponding non-mass transfer case. This indicates that breakage becomes the dominating mechanism and leads to substantial increase in surface area even in the presence of solid dissolution. The rapid size decrease enabled by the combined effects of mass transfer and sonication may have created smaller particles which however did not dissolve as much as the larger ones as the former individually had smaller surface areas. These particles may have accumulated in the moderate and smaller size ranges of the dispersion to a larger extent and contributed to a higher surface area. At the end of 6 min of sonication, considerable presence of coarse particles in the non-mass transfer case was observed (Fig. 5a) whereas a substantial density of particles in the intermediate and fine size range was evident under mass transfer conditions (Fig. 5b). This trend continues even until 9 min of sonication. At the end of 9 min, Fig. 6a shows significant presence of coarse particles in the non-mass transfer case. However, Fig. 6b shows substantial density of particles in the intermediate and fine size range under mass transfer conditions.

Even after 30 min of sonication, the presence of larger particles in the non-mass transfer case is considerably more significant than in the mass transfer case even though solid dissolution had ceased in the latter. This shows that there are more particles in the smallest size range under mass transfer conditions creating more surface area than in the non-mass transfer case. A major fraction of

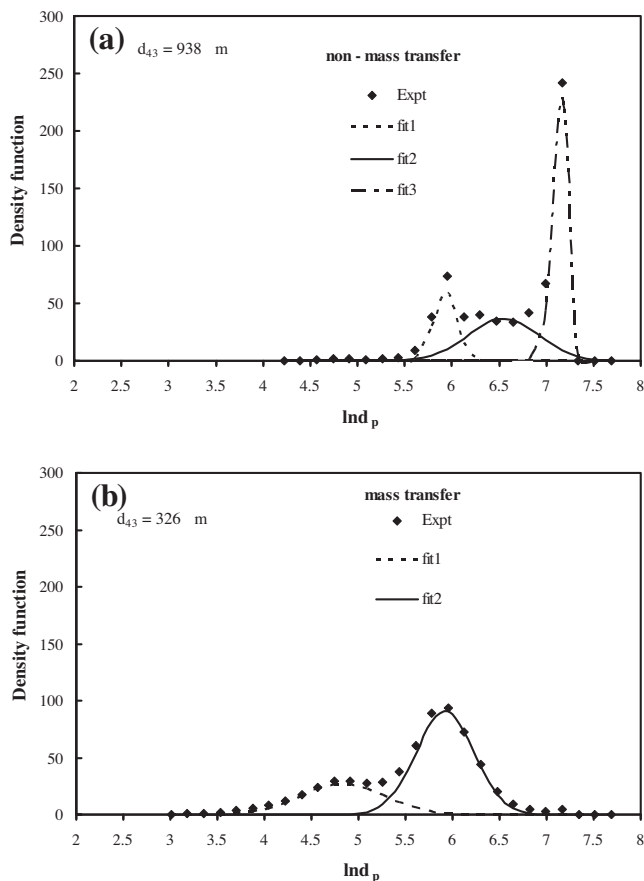


Fig. 5. Comparison of experimental data and individual lognormal models of probability density functions for System 1 after 6 min of sonication at 70% power level setting under (a) non-mass transfer and (b) mass transfer conditions.

the particles was in the size range between 2 and 90 μm after 30 min of sonication at 70% power level setting in the mass transfer case. On the other hand, for the same power level setting, non-mass transfer conditions yielded particles mainly in the size range between 12 and 245 μm after 30 min of sonication. The higher power dissipation at 70% (115 W/L) when compared to what was obtained at 50% (69 W/L) led to considerable particle breakage and creation of greater surface area.

3.2.3. 50% power level setting for System 2

Under mass transfer conditions, the loss of surface area from solid dissolution counterbalances the gain of surface area by particle breakage in the first phase of the particle size reduction process. This explains the slow initial increase in the surface area for the mass transfer case shown in Fig. 4c. Under non-mass transfer conditions, the absence of particle dissolution led to higher surface area values. System 2 reached near 99% saturation conditions after 15 min at which point the energy dissipation was 66 kJ/kg (Table 3). The energy dissipation of 105 kJ/kg corresponds to 23.7 min. Once the inhibiting effects of mass transfer in reducing area was no longer important at energy dissipation levels close to 105 kJ/kg, cavitation could increase the surface area faster.

As shown in Table 3, the d_{43} of System 2 is 760 μm after 15 min when sonicated at a power level setting of 50% under mass transfer conditions. At this juncture, most of the particles were distributed around a mean particle size of 910 μm . A total sonication time of 30 min at 50% power level setting could only reduce the d_{43} to 597 μm . Even at this point in time, there existed a significant fraction of coarsest particles distributed around the size range of

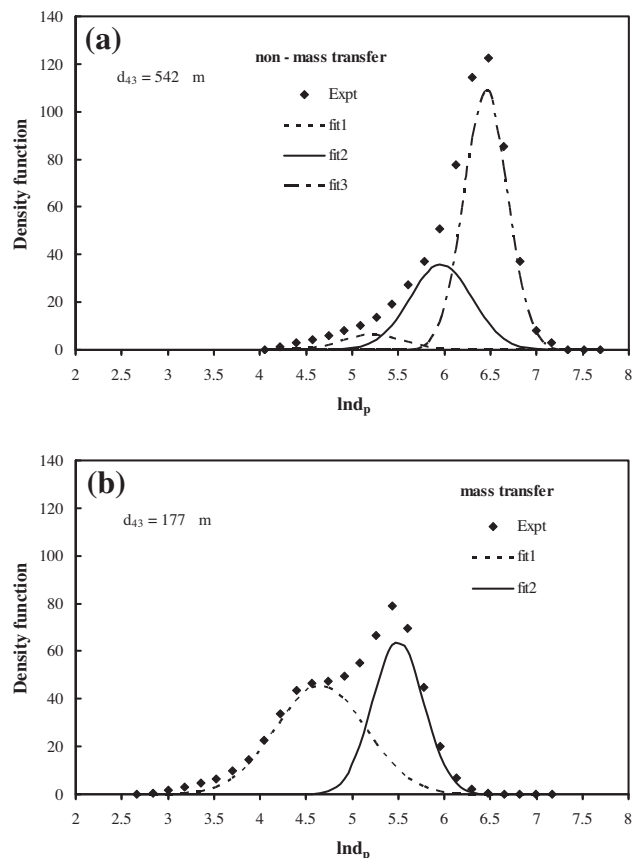


Fig. 6. Comparison of experimental data and individual lognormal models of probability density functions for System 1 after 9 min of sonication at 70% power level setting under (a) non-mass transfer and (b) mass transfer conditions.

870 μm ($\ln(d_p) = 6.77$). This clearly illustrates that particle breakage was rather mild for System 2 once it reached saturation conditions at 50% power level setting. This is directly reflected in a slow rise of SA at these conditions (Fig. 4c).

3.2.4. 70% power level setting for System 2

It may be seen from Fig. 4d that in the mass transfer case, there is also a region of slow increase in SA between EM values of 58 kJ/kg and approximately 105 kJ/kg after which the increase in SA is considerable with respect to the ultrasonic energy supplied. System 2 took 9 min to reach saturation conditions at 70% power level setting at which point the energy dissipated was 58 kJ/kg. The specific energy dissipation 105 kJ/kg corresponds to 16.2 min at 70% power level setting. There appears to be some time lag for further surface area increase to take place once System 2 attained near saturation conditions, as evident at both 50% and 70% power level settings under mass transfer conditions as shown in Fig. 4c and d. Significantly higher surface areas, obtained in systems where mass transfer occurred initially, at higher energy levels may be attributed to the presence of a significant proportion of particles present in the lower size range. This may be clearly seen from Fig. 7 for System 2 after 30 min of sonication under mass transfer conditions. It appears that as long as mass transfer was occurring, there was some loss in surface area due to dissolution, but also smaller particles were being simultaneously produced. Once the solid dissolution stopped in the mass transfer situation, there were many smaller particles left over in the dispersion. In the absence of mass transfer, the particles, though not losing surface area due to solid dissolution, still remained fairly large during the sonication process (Fig. 7). In this case, the particles were breaking at a nearly

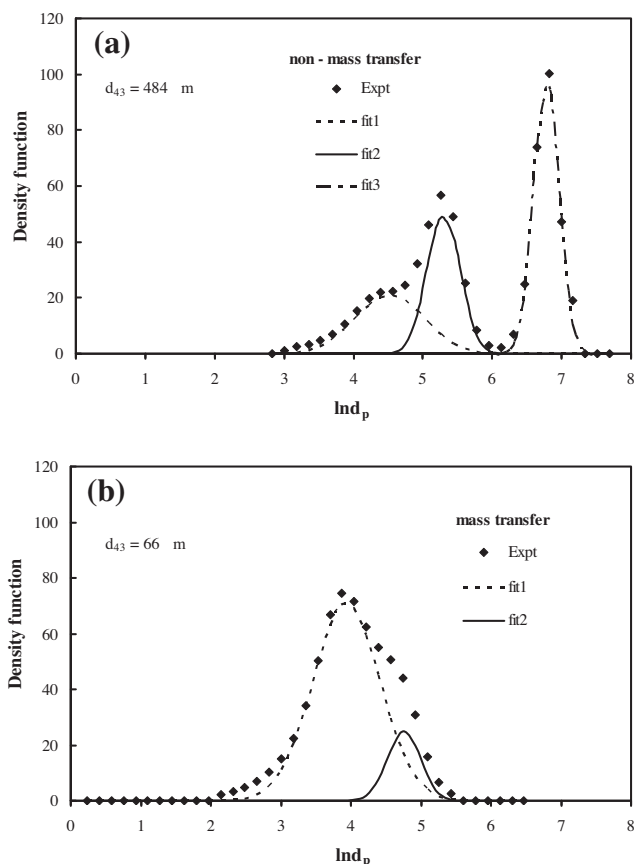


Fig. 7. Comparison of experimental data and individual lognormal models of probability density functions for System 2 after 30 min of sonication at 70% power level setting under (a) non-mass transfer and (b) mass transfer conditions.

uniform rate as may be seen in the consistent but gradual increase in the surface area (Fig. 4d).

In Fig. 3b, the average d_{43} was decreasing only slowly in the non-mass transfer case even at this high power level setting, while it decreased more rapidly at the same power level setting in the mass transfer case (Fig. 2b).

Sonication at 70% power level setting was able to break the particles in System 2 even after reaching saturation conditions. The d_{43} at near saturation conditions obtained with this power level setting was 438 μm (Table 3) and after a total sonication time of 30 min the d_{43} was 66 μm (Fig. 2b). Hence there was a remarkable rise in SA for this system after it reached saturation conditions when treated at 70% power level setting (Fig. 4d) when compared to 50% power level setting (Fig. 4c).

It is, however, not that easy for cavitation triggered events such as microjets to be very effective when the particle sizes are small.

Microjets fragment the particles present in the vicinity and are responsible for pitting and erosion of solid surface [7]. The velocities of these microjets were estimated to be of the order of 100 m/s [24]. However there seems to be a limit for the microjet induced effects. Alex et al. [25] observed that when particles are smaller than the cavitating bubble they do not influence cavity collapse while particles larger than cavitating bubble sizes will act as a surface for microjet formation. Suslick and Price [26] observed that when the particles are smaller than 200 μm in size, the microjetting phenomenon ceases to be effective at ultrasound frequencies in the order of 20 kHz and the inter-particle collisions with great force induced by shockwaves becomes important. Shockwaves produced as a result of symmetric collapse of the cavitation bubbles will result in microstreaming which enhances the rate of mass transfer [7]. Further, shockwaves are capable of causing fracture to the solid surface [5]. The particle velocities created by shockwaves depend upon particle size, solution viscosity, slurry density, etc. Larger particles will be only minimally accelerated by cavitation induced shockwaves. When the viscosity of the solution increases, the velocities of inter-particle collisions in the liquids decrease [27]. Hence there is a time lag and more energy has to be input into the system for the smaller particles to be eventually broken with consequent increase in the surface area. However, once these particles are broken by repeated effects of the cavitating bubbles, the surface area increased significantly.

Typical distributions shown in Figs. 5–7 indicate a multimodal form. The log-normal fit details of these distributions are given in Table 6. Usually, multimodal particle size distributions observed in ultrasound assisted particle breakage studies may be attributed to a combination of factors [5,28–31]. Bimodal particle size distributions arise due to solid characteristics and breakage forces [32]. Erosion was found to be responsible for the growth of secondary distribution of fine particles [29]. In addition to the primary shears from microjets and inter-particle collisions which fragment particles, there might be other kinds of damage to the particles which result in the formation of fine particles. Weak spots on the solid surface, outer corners and edges are susceptible for getting chipped off and/or eroded and thus may contribute for a secondary distribution. If one of the mechanisms causing the secondary distribution is extremely prevailing, then a third distribution begins [32]. This implies that the particles belonging to the second distribution may get further eroded to form the third distribution.

3.3. Estimation of the intrinsic mass transfer coefficient

Usually in ultrasound experiments involving mass transfer, the volumetric mass transfer coefficient ($k_c a$) is treated as a lumped parameter for the process under investigation [33]. Kannan and Pathan [34] reported intensification due to ultrasound on intrinsic mass transfer coefficients as the surface area of the rotating benzoic acid solid cylinder was nearly constant. The problem is more

Table 6
Fitted lognormal parameters for mass transfer (MT) case depicted in Figs. 5–7.

System	Ultrasonic power level setting (%)	Sonication time (min)	Fit ID	Non-mass transfer conditions				Mass transfer conditions			
				A_i (%)	B_i	C_i	R^2	A_i (%)	B_i	C_i	R^2
1	70	6	Fit 1	18.61	0.122	5.925	0.994	30.47	0.446	4.838	0.998
			Fit 2	34.01	0.369	6.548		69.53	0.305	5.921	
			Fit 3	47.38	0.069	7.126		–	–	–	
1	70	9	Fit 1	5.42	0.326	5.218	0.999	55.84	0.489	4.659	0.998
			Fit 2	30.44	0.338	5.965		44.16	0.271	5.501	
			Fit 3	64.14	0.234	6.450		–	–	–	
2	70	30	Fit 1	25.81	0.492	4.525	0.994	85.38	0.480	3.936	0.996
			Fit 2	29.89	0.242	5.298		14.62	0.235	4.757	
			Fit 3	44.30	0.181	6.783		–	–	–	

Table 7
Predicted values of the intrinsic mass transfer coefficient (k_c) for different ultrasonic experimental conditions.

Solid–liquid system	Ultrasonic power level setting (% of maximum)	Power dissipated (W/L)	Intrinsic mass transfer coefficient (k_c) (cm/min)
Benzoic acid–distilled water	50	68.5	0.216
	70	115.1	0.527
Benzoic acid–24% (w/w) aqueous glycerol	50	77.9	0.340
	70	114.5	0.790

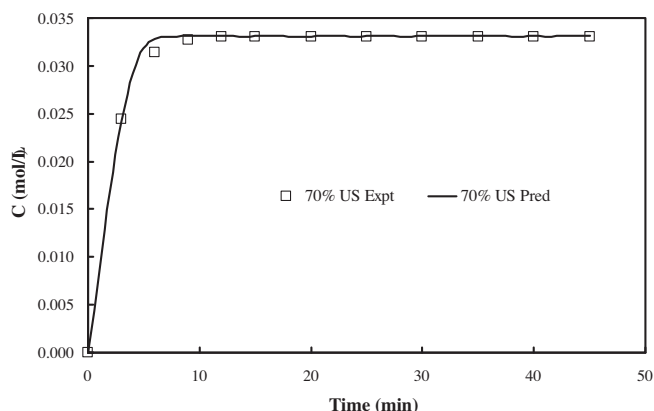


Fig. 8. Comparison of predicted and experimental concentrations for System 1 at 70% ultrasonic power level setting assuming a constant intrinsic mass transfer coefficient.

difficult in dispersed systems. However, in this work, the intrinsic mass transfer coefficient (k_c), could be obtained from the volumetric mass transfer coefficient ($k_c a$) as the surface area data were measured. The availability of k_c also enables the estimation of Sherwood number. The analysis was divided into two parts. In the first part, the intrinsic mass transfer coefficient (k_c) was assumed to be a constant lumped parameter and independent of batch dissolution kinetics. This represents a first approximation and is discussed below (Section 3.3.1). In the subsequent analysis (Section 3.3.2), the lumped parameter assumption is relaxed and the intrinsic mass transfer coefficient is allowed to vary.

3.3.1. Constant intrinsic mass transfer coefficient (k_c)

The intrinsic mass transfer coefficient (k_c) was taken as constant at each experimental condition. The empirical expressions obtained for surface area as a function of ultrasonic energy per unit mass (Eq. (6)) were substituted in Eq. (1) and the resulting expression was numerically integrated using the methodology given in Section 2.5.

The estimated values of the intrinsic mass transfer coefficient (k_c) are summarized in Table 7. It can be seen from this Table that the intrinsic mass transfer coefficient (k_c) increases as the power dissipated increases. This may be attributed to the enhanced microturbulence in the solid–liquid film prevailing at higher power level setting. This increase is observed in both the systems investigated. The concentration values predicted are compared with those obtained experimentally in Fig. 8 for System 1 treated at 70% power level setting.

3.3.2. Intrinsic mass transfer coefficient (k_c) accounting for variation in particle size

Zanwar and Pangarkar [35] observed that the conventional definition of Reynolds number in terms of a length and velocity scales is not easy in ultrasonic applications as there is no information on the nature of the turbulence. In well agitated dispersions, the solid–liquid mass transfer is affected in a complicated manner by

bulk liquid turbulence, particle size and solute diffusivity, liquid viscosity, etc. [36]. In the present work, the possible candidates for length scale are ultrasonic probe tip diameter, vessel diameter or average particle diameter. The ultrasound probe diameter is not a standard parameter which has a definite geometric scaling rule with the vessel dimensions as in a standard mixing vessel. The particle representative (i.e., mean) diameter is a more logical choice as the particles movement relative to the liquid in the presence of ultrasound influences the convective mass transfer coefficient. Here, d_{43} is considered as the representative diameter. Even though this parameter changes with time due to particle breakage and dissolution (Fig. 2), this has been measured in this work. Hence the particle size distribution not only influences the interfacial area of mass transfer but also plays an important role in defining the intrinsic mass transfer coefficient itself. Further, ultrasound velocity scales are difficult to quantify and may vary with system properties and power dissipation levels. Further, different particles may move with different velocities in the dispersion under the influence of ultrasound. Hence it is preferable if the ultrasound power dissipation itself may be introduced in the Sherwood number correlation for mass transfer rather than a velocity scale. This approach has been used previously by Kannan and Pathan [34]. The equivalent stirrer speed approach introduced by Simon et al. [37] for ultrafiltration applications was also tried in this work to correlate the intrinsic mass transfer coefficients in the presence of ultrasound. However, the problem of suitable choice of length dimensions in the Reynolds number term as discussed above arose. Further, the fitted equivalent stirring speed values were very high in the order of few thousands and the confidence intervals of this fitted parameter were very broad. Hence this approach of equivalent stirrer speed was not pursued further in our work.

After the above attempt, it was decided to test the Kolmogoroff's method as suggested by Zanwar and Pangarkar [35]. Sanger and Deckwer [38] suggested this approach to circumvent the modeling approach from the need to know the relative velocity. Gogoi and Dutta [36] also favored using this approach in three phase sparged reactors where benzoic acid dissolution in turbulent liquid medium was analyzed. The agitation in this application was provided by aeration at different velocities. They observed that the Reynolds number may be described in terms of some measurable macroscopic quantities. This approach is widely popular in modeling mass transfer systems and has been considered for instance by Kawase and Moo-Young [39] and Aravamudan and Baird [40]. The energy dissipation term also is introduced quite naturally in combination with the mixing length (l) term to define the equivalent velocity scale as shown below. The velocity scale (u) is given by

$$u = (\varepsilon l)^{1/3} \quad (8)$$

Since the Reynolds number is defined by

$$\text{Re} = \frac{lu}{\nu} \quad (9)$$

this leads to the following equation after substituting d_{43} for the characteristic particle dimension l

$$\text{Re}_{\text{US}} = \frac{d_{43}^{4/3} \varepsilon^{1/3}}{\nu} \quad (10a)$$

This form of the Reynolds number was chosen as the particle's length dimension was greater than $(\nu^3/\varepsilon)^{1/4}$. For particle dimension smaller than $(\nu^3/\varepsilon)^{1/4}$, an alternative form of Re_{US} is used [36]:

$$\text{Re}_{\text{US}} = \frac{d_{43} \varepsilon^{1/4}}{\nu^{3/4}} \quad (10b)$$

For example, even if the average particle size is in the order of $10^2 \mu$ ($500 \mu\text{m}$ during mass transfer would be a very conservative estimate), this was greater than the length scale obtained ($10 \mu\text{m}$) as estimated by $(\nu^3/\varepsilon)^{1/4}$ for the present systems under investigation. The Sherwood number in the presence of ultrasound is defined as follows:

$$\text{Sh}_{\text{US}} = \alpha(\text{Re}_{\text{US}})^\beta (\text{Sc})^\gamma \quad (11a)$$

$$\text{where } \text{Sh}_{\text{US}} = \frac{k_{\text{US}} d_{43}}{D_{\text{AB}}} \quad (11b)$$

Since the local Sherwood number is difficult to measure along the particle surface, its average value is required. However, it cannot be calculated for each particle in the dispersion. Hence, the average Sherwood number for the entire dispersion at a given instant is characterized in terms of instantaneous average particle size (d_{43}) in the dispersion. This length scale is used both in the Sherwood number correlation as well as in the Reynolds number group. The exponents of the Sherwood number correlation (Eq. (11a)) were obtained in the following manner.

The variations of d_{43} with time as shown in Figs. 2a and b for different systems and different conditions were each fitted with a suitable piecewise polynomial expression with regression coefficient of practically unity. The resulting polynomial expressions for d_{43} were embedded in the correlation for Sherwood number (Eq. (11)). Now the Sherwood number or equivalently the intrinsic mass transfer coefficient also becomes time dependent as it is a function of the time dependent d_{43} . Next, the Sherwood number correlation form (Eq. (11a)) and the surface area correlations (Eq. (6)) were embedded in Eq. (1). The parameter fitting was carried out as described in Section 2.5 to yield the exponents of the Sherwood number correlation as shown in Eq. (12).

$$\text{Sh}_{\text{US}} = 0.6732 \text{Re}_{\text{US}}^{0.4360} \text{Sc}^{0.3366} \quad (12)$$

Typically, in mass transfer correlations, the exponent of Schmidt number in boundary layer controlled situations is 1/3. In the present work, the exponent of the Schmidt number (γ) is included along with α and β for estimation in the nonlinear estimation of parameters. The exponent of Reynolds number is typically 0.5 or 0.8 in conventional processes i.e., where ultrasound was absent. However, Zanwar and Pangarkar [35] observed the exponent for Re to be only 0.217 and concluded to be due to low utilization of ultrasonic power.

From Eqs. ((11b) and (12)), the intrinsic mass transfer coefficient may be obtained as a function of time, for different systems and power dissipations, using the same piecewise polynomial expressions for d_{43} obtained as described above. Fig. 9 depicts the variation of the intrinsic mass transfer coefficient as a function of normalized time for System 1 at 50% and 70% ultrasonic power level settings. The time of sonication was divided by the time taken by the solid-liquid system to attain saturation to get the normalized time. The solid and dashed lines correspond to the values of the intrinsic mass transfer coefficient (k_c) obtained from the lumped system approach previously outlined in Section 3.3.1. The trends with symbols represent the values of k_c obtained by accounting for the change in particle size (d_{43}). It may be easily perceived from this figure that there exists a significant difference

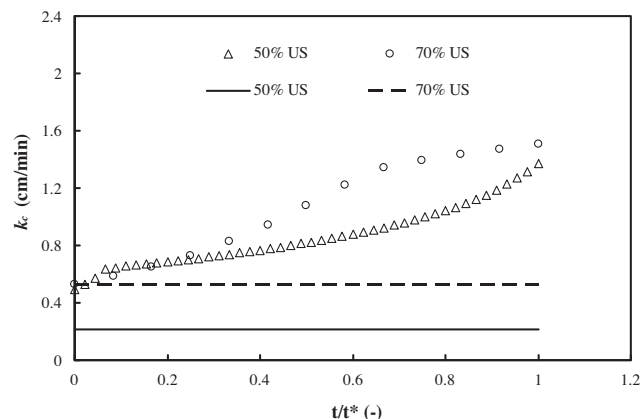


Fig. 9. Variation of intrinsic mass transfer coefficient as a function of dimensionless time for System 1 at different ultrasonic power level settings based on d_{43} .

in the magnitude of k_c predicted by these two approaches. The variation in k_c for System 1 was found to increase with an increase in the power level setting for both the approaches. It may be observed from Fig. 9 that the increase in k_c is rapid at 70% power level setting. This may be due to higher effect of microturbulence in case of 70% power level setting when compared to 50% power level setting. Higher power level setting leads to enhanced particle breakage and hence more number of smaller particles. The microturbulence occurring in the solid-liquid interface of each of these numerous smaller particles may contribute to augment the overall k_c of the dispersion.

The variation of k_c for System 2 is illustrated in Fig. 10. At 50% power levels, the interfacial area for mass transfer did not change significantly during most of the run (Fig. 4c, MT conditions). Hence the variable intrinsic mass transfer coefficient does not vary too much from the value predicted by the lumped parameter model. The significant variation in k_c observed in case of 70% power level setting System 1 is not evident for System 2 at the same 70% power level setting. In fact, the intrinsic mass transfer coefficients are even somewhat comparable with the mass transfer coefficients obtained at 50% power level settings (Fig. 10). This may be due to the higher viscosity of System 2. The constant (i.e., lumped) k_c approach under predicted the k_c values for System 1 and over predicted for System 2 at all ultrasonic power level settings used. Actually, the particle size distribution's variation with time not only influences both d_{43} which appears in the Reynolds number and Sherwood number terms in Eq. (11) but also influences the surface area evolution with time for mass transfer. Hence the

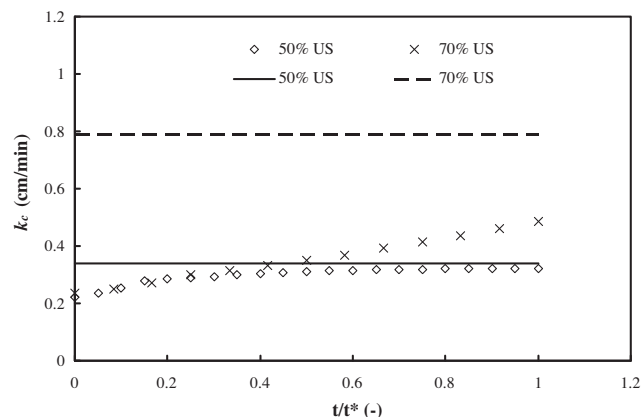


Fig. 10. Variation of intrinsic mass transfer coefficient as a function of dimensionless time for System 2 at different ultrasonic power level settings based on d_{43} .

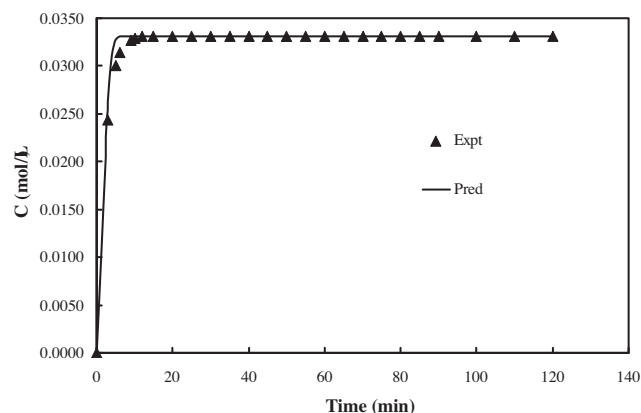


Fig. 11. Comparison of predicted and experimental concentration for System 1 at 70% ultrasonic power level setting based on variable k_c approach.

trends involving intrinsic variable k_c when associated with significant changes in d_{43} and surface area are rather complex.

From Figs. 9 and 10, it may be seen that the variable mass transfer coefficient approach predicts higher intrinsic mass transfer coefficients for the pure water based System 1 than the glycerol based System 2. This would be usually expected on the basis of higher diffusivity of System 1 than System 2 as shown in Table 1. However, the lumped mass transfer coefficients approach, as indicated by the straight lines of Figs. 9 and 10, shows opposite trends. This approach assumes a constant intrinsic mass transfer coefficient that is invariant with time and therefore this approach may be treated as a first approximation only as was already mentioned in Section 3.3. Hence, due to the significant variations in the predictions by the lumped intrinsic mass transfer coefficients it is recommended to use the variation of particle size to predict the time-dependent values of k_c if the particle size data at various sonication times are available. Fig. 11 shows the typical experimental and predicted concentration trends obtained for System 1 by using variable k_c approach when operated at 70% power level setting. For this case, the predictions are slightly higher than the experimental values.

Another important consideration here is the use of appropriate particle size distribution and surface area information when designing ultrasonically intensified mass transfer equipment. The Sherwood number correlations used in the design must incorporate average particle size diameter and interfacial area obtained under mass transfer conditions. There is wide disparity in these data as discussed earlier, between the mass transfer and non-mass transfer runs. Hence, the data generated under non-mass transfer conditions, may not be used for mass transfer applications. This is somewhat similar to studies in extraction equipment where the drop hydrodynamics prevailing under mass transfer conditions are distinct from the hydrodynamics encountered under non-mass transfer conditions. In such cases, the solute transfer from the dispersed phase to continuous phase induces coalescence of drops due to interfacial tension gradients thereby leading to much lower surface areas than those obtained in conditions where the drops were not induced to coalesce [41,42]. Hence correlations developed for dispersed phase holdup and interfacial area in the absence of solute transfer cannot be automatically extended to cases where mass transfer is also present.

4. Summary

The major findings from this work are listed below

- A detailed study on the evolution of surface area of benzoic acid particles with time has been made under both mass transfer and non-mass transfer conditions.
- The evolution of particle size distributions and the average diameter (d_{43}) has been compared for both mass transfer and non-mass transfer conditions.
- The ultrasonic energy input required to saturate benzoic acid particles in aqueous solvents has been identified.
- A Sherwood number correlation has been proposed to estimate ultrasound induced intrinsic mass transfer coefficient. The system properties and ultrasound power input levels are used in this correlation. This correlation will be useful in the design of commercial ultrasonic process equipment used for simultaneous particle size reduction and dissolution.

5. Conclusions

The multimodal particle size distributions obtained with ultrasound induced particle breakage could be described in terms of a combination of lognormal statistical distributions. The variation of De Brouckere mean diameter (d_{43}) as a function of ultrasonic energy input and sonication time were investigated both under mass transfer and non-mass transfer conditions. This study clearly demonstrates the intensification provided by ultrasound in creating smaller particle sizes and hence enabling greater surface area especially at higher ultrasonic power levels.

The surface area created as a result of ultrasound-assisted particle breakage and dissolution for each system investigated was quantified with respect to ultrasonic energy per unit mass for both the mass transfer and non-mass transfer cases. Under mass transfer conditions, both the solid–liquid systems studied reached near saturation concentrations in presence of ultrasound at an ultrasonic energy input per unit mass of about 60 kJ/kg. Further, the estimation of interfacial area could delineate the intrinsic mass transfer coefficient from the volumetric mass transfer coefficient and aid in the development of a design correlation for Sherwood number. The intrinsic mass transfer coefficients for both the solid–liquid systems studied were estimated numerically under sonicated conditions by two methods viz. constant k_c approach and varying k_c approach. The variable k_c approach provided an insight into the temporal effect of ultrasound on the intrinsic mass transfer coefficient.

Initial solute transfer before saturation was found to create particle size distributions that were considerably different from those obtained in the complete absence of solute transfer. This has implications on the temporal variation of the average particle size and the surface area. Hence, in the design of ultrasonically intensified mass transfer equipment, Sherwood number correlations ought to be based on particle size distribution data obtained under solute transfer conditions.

Acknowledgement

The authors are grateful to Prof. Paramanand Singh, I.I.T. Madras for providing the particle size analyzer facility.

References

- L.H. Thompson, L.K. Doraiswamy, Sonochemistry: science and engineering, Industrial and Engineering Chemistry Research 38 (1999) 1215–1249.
- C. Leonelli, T.J. Mason, Microwave and ultrasonic processing: now a realistic option for industry, Chemical Engineering and Processing 49 (2010) 885–900.
- L.H. Thompson, L.K. Doraiswamy, The rate enhancing effect of ultrasound by inducing supersaturation in a solid–liquid system, Chemical Engineering Science 55 (2000) 3085–3090.
- D.K. Sandilya, A. Kannan, Effect of ultrasound on the solubility limit of a sparingly soluble solid, Ultrasonics Sonochemistry 17 (2010) 427–434.
- Y. Lu, N. Riyanto, L.K. Weavers, Sonolysis of synthetic sediment particles: particle characteristics affecting particle dissolution and size reduction, Ultrasonics Sonochemistry 9 (2002) 181–188.

- [6] N. Ratoarinoro, A.M. Wilhelm, J. Berlan, H. Delmas, Effects of ultrasound emitter type and power on a heterogeneous reaction, *The Chemical Engineering Journal* 50 (1992) 27–31.
- [7] L.C. Hagenson, L.K. Doraiswamy, Comparison of the effects of ultrasound and mechanical agitation on a reacting solid–liquid system, *Chemical Engineering Science* 53 (1998) 131–148.
- [8] V. Sivakumar, G. Swaminathan, P.G. Rao, C. Muralidharan, A.B. Mandal, T. Ramasami, Use of ultrasound in leather processing industry: effect of sonication on substrate and substances – new insights, *Ultrasonics Sonochemistry* 17 (2010) 1054–1059.
- [9] J.L. Pérez-Rodríguez, F. Carrera, J. Poyato, L.A. Pérez-Maqueda, Sonication as a tool for preparing nanometric vermiculite particles, *Nanotechnology* 13 (2002) 382–387.
- [10] F. Franco, L.A. Pérez-Maqueda, J.L. Pérez-Rodríguez, The effect of ultrasound on the particle size and structural disorder of a well-ordered kaolinite, *Journal of Colloid and Interface Science* 274 (2004) 107–117.
- [11] N. Ratoarinoro, F. Contamine, A.M. Wilhelm, J. Berlan, H. Delmas, Activation of a solid–liquid chemical reaction by ultrasound, *Chemical Engineering Science* 50 (1995) 554–558.
- [12] W.L. McCabe, J.C. Smith, P. Harriott, *Unit Operations of Chemical Engineering*, fifth ed., McGraw-Hill Inc., New York, 1993.
- [13] T. Allen, *Powder Sampling and Particle Size Determination*, Elsevier, Amsterdam, 2003.
- [14] C.J.D.E. Ruiter, F. Oeseburg, A comparison of parameter estimation procedures for experimental bimodal lognormal particle size distributions and grouped data, *Journal of Aerosol Science* 18 (1987) 431–444.
- [15] R. Parthasarathy, N. Ahmed, Bubble size distribution in a gas sparged vessel agitated by a Rushton turbine, *Industrial and Engineering Chemistry Research* 33 (1994) 703–711.
- [16] A. Voutilainen, J.P. Kaipio, Estimation of time-varying aerosol size distributions – exploitation of modal aerosol dynamical models, *Journal of Aerosol Science* 33 (2002) 1181–1200.
- [17] R.F. Liu, C.-K. Hu, L. Gignac, J.M.E. Harper, J. Lloyd, X.-H. Liu, A.K. Stamper, Effects of failure criteria on the lifetime distribution of dual-damascene Cu line/via on W, *Journal of Applied Physics* 95 (2004) 3737–3744.
- [18] C.M. Tan, N. Raghavan, A bimodal three-parameter lognormal mixture distribution for electromigration failure analysis, *Thin Solid Films* 516 (2008) 8804–8809.
- [19] M. Meier, E. John, D. Wieckhusen, W. Wirth, W. Peukert, Generally applicable breakage functions derived from single particle comminution data, *Powder Technology* 194 (2009) 33–41.
- [20] L.-S. Fan, C. Zhu, *Principles of Gas–Solid Flows*, Cambridge University Press, Cambridge, 1998.
- [21] L. Ma, R.K. Hanson, Measurement of aerosol size distribution functions by wavelength-multiplexed laser extinction, *Applied Physics B: Lasers and Optics* 81 (2005) 567–576.
- [22] K. Krishnamoorthy, *Handbook of statistical distributions with applications*, Chapman & Hall/CRC, Boca Raton, 2006.
- [23] W.A. Sowa, Interpreting mean drop diameters using distribution moments, *Atomization and Sprays* 2 (1992) 1–15.
- [24] K.S. Suslick, S.J. Doktycz, E.B. Flint, On the origin of sonoluminescence and sonochemistry, *Ultrasonics* 28 (1990) 280–290.
- [25] C.–C.T. Alex, N.K. Goh, L.S. Chia, Effects of particle morphology on ultrasonic-induced cavitation mechanisms in heterogeneous systems, *Journal of the Chemical Society, Chemical Communications* 1 (1995) 201.
- [26] K.S. Suslick, G.J. Price, Applications of ultrasound to materials chemistry, *Annual Review of Materials Science* 29 (1999) 295–326.
- [27] S.J. Doktycz, K.S. Suslick, Interparticle collisions driven by ultrasound, *Science* 247 (1990) 1067–1069.
- [28] K.A. Kusters, S.E. Pratsinis, S.G. Thoma, D.M. Smith, Ultrasonic fragmentation of agglomerate powders, *Chemical Engineering Science* 48 (1993) 4119–4127.
- [29] K.A. Kusters, S.E. Pratsinis, S.G. Thoma, D.M. Smith, Energy-size reduction laws for ultrasonic fragmentation, *Powder Technology* 80 (1994) 253–263.
- [30] U. Teipel, K. Leisinger, I. Mikonsaari, Comminution of crystalline material by ultrasonics, *International Journal of Mineral Processing* 74S (2004) S183–S190.
- [31] V. Raman, A. Abbas, Experimental investigations on ultrasound mediated particle breakage, *Ultrasonics Sonochemistry* 15 (2008) 55–64.
- [32] P.S. Roller, Statistical analysis of size distribution of particulate materials, with special reference to bimodal and frequency distributions: correlation of quartile with statistical values, *Journal of Physical Chemistry* 45 (1941) 241–281.
- [33] M.V. Dagaonkar, H.J. Heeres, A.A.C.M. Beenackers, V.G. Pangarkar, Investigation of enhanced gas adsorption by adsorptive bucky balls in a multiphase slurry reactor in the presence and absence of ultrasound, *Industrial and Engineering Chemistry Research* 41 (2002) 1496–1503.
- [34] A. Kannan, S.K. Pathan, Enhancement of solid dissolution process, *Chemical Engineering Journal* 102 (2004) 45–49.
- [35] S.S. Zanwar, V.G. Pangarkar, Solid–liquid mass transfer in packed beds: enhancement due to ultrasound, *Chemical Engineering Communications* 68 (1988) 133–142.
- [36] N.C. Gogoi, N.N. Dutta, Empirical approach to solid–liquid mass transfer in a three-phase sparged reactor, *Fuel Processing Technology* 48 (1996) 145–157.
- [37] A. Simon, L. Penpenic, N. Gondrexon, S. Taha, G. Dorange, A comparative study between classical stirred and ultrasonically-assisted dead-end ultrafiltration, *Ultrasonics Sonochemistry* 7 (2000) 183–186.
- [38] P. Sängler, W.-D. Deckwer, Liquid–solid mass transfer in aerated suspensions, *The Chemical Engineering Journal* 22 (1981) 179–186.
- [39] Y. Kawase, M. Moo-Young, Solid–turbulent fluid heat and mass transfer: a unified model based on the energy dissipation rate concept, *The Chemical Engineering Journal* 36 (1987) 31–40.
- [40] K. Aravamudan, M.H.I. Baird, Effect of unstable density gradients on back-mixing in a reciprocating plate column, *AIChE Journal* 42 (1996) 2128–2140.
- [41] K. Aravamudan, M.H.I. Baird, Effects of mass transfer on the hydrodynamic behavior of a Karr reciprocating plate column, *Industrial and Engineering Chemistry Research* 38 (1999) 1596–1604.
- [42] K. Aravamudan, M.H.I. Baird, Formation of tailed drops in liquid–liquid extraction, *Chemical Engineering Science* 55 (2000) 1029–1031.